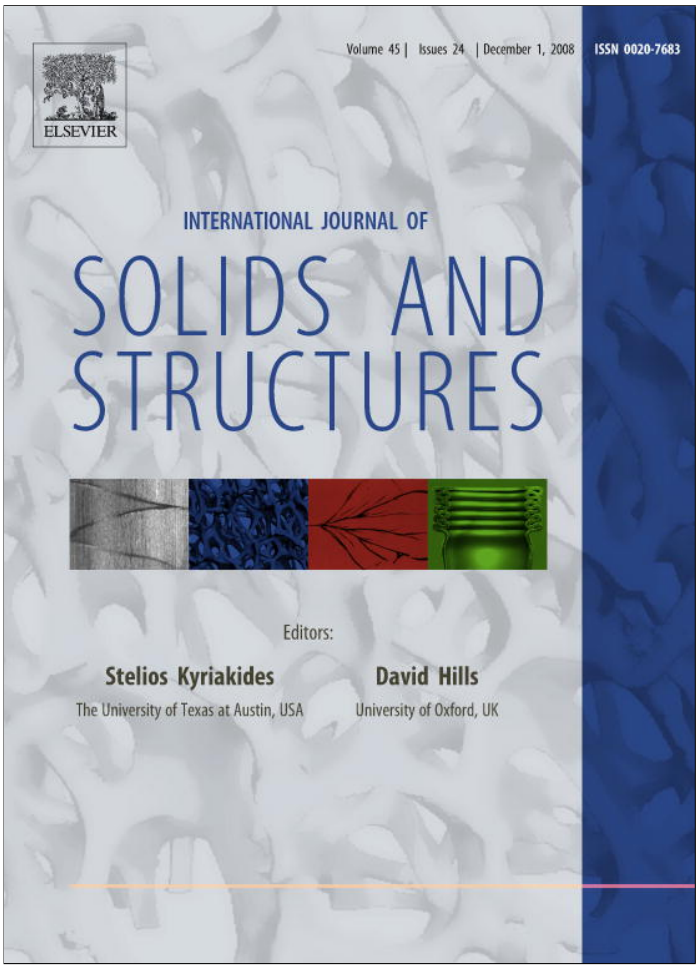

International Journal of Solids and Structures 45 (2008) 6034–6044

Contents lists available at ScienceDirect

International Journal of Solids and Structures

journal homepage: www.elsevier.com/locate/ijsolstr

Cracks in rubber

P. Trapper, K.Y. Volokh *

Faculty of Civil and Environmental Engineering, Technion – Israel Institute of Technology, Haifa 32000, Israel

ARTICLE INFO

Article history:
Received 15 April 2008
Received in revised form 6 July 2008
Available online 31 July 2008

Keywords:
Rubber
Crack
Fracture
Failure
Hyperelasticity
Softening

ABSTRACT

The onset of crack propagation in rubber is studied computationally by using the softening hyperelasticity approach. The basic idea underlying the approach is to limit the capability of a material model to accumulate energy without failure. The latter is done by introducing a limiter for the strain energy density, which results from atomic/molecular considerations and can be interpreted as the average bond energy or the failure energy. Including the energy limiter in a constitutive description of material it is possible to enforce softening and, consequently, allow tracking the onset of structural instability corresponding to the onset of material failure. Specifically, initiation of crack propagation is studied in the case of a thin sheet of a rubber-like solid under the hydrostatic tension. The large deformation neo-Hookean material model enhanced with the energy limiter is used for finding the critical tension corresponding to the onset of static instability of the sheet, i.e. the onset of fracture propagation. The influence of the crack sharpness and length on the critical load is analyzed. It is found that material is sensitive to the crack sharpness when the shear modulus is significantly greater than the average bond energy. The sensitivity declines when the value of the shear modulus approaches the value of the failure energy. Roughly speaking, softer materials are less sensitive to cracks than more brittle materials where the brittleness is defined as a ratio of the shear modulus to the failure energy. It is also found that the critical tension is proportional to the inverse square root of the crack length for more brittle materials. The latter means that the Griffith theory based on the linearized elasticity is also applicable to softer materials undergoing large deformations. Unfortunately, the applicability of the Griffith theory is restricted to cracks with equivalent sharpness only.

1. Introduction

Large deformations make analysis of cracks in rubber difficult. There were very few studies accounting for large deformations in rubber-like materials: Knowles and Sternberg (1973, 1983), Knowles (1977, 1981), Herrmann (1989), Geubelle and Knauss (1994a,b,c), Geubelle (1995). These studies aimed at clarifying the asymptotic structure of the deformation and stress fields near the crack tip in various hyperelastic materials undergoing finite strains. The cited works showed that the geometrical and material nonlinearities may have a pronounced effect on the fracture predictions in rubber-like solids.

Another line of studying cracks in rubber stemmed from the physical observations of the influence of the rubber viscosity on crack propagation. The works in this direction have been recently reviewed by Persson et al. (2005). It is interesting that the works considered in the cited review are based on the linear elastic fracture mechanics (LEFM) and its linear viscoelasticity extension for rubbers – see also Gent (2001). Thus, both the material and geometrical nonlinearities are ignored. Such ignorance is probably justified when rubber is in the glassy state and it behaves like a hard quasi-brittle material.

* Corresponding author. Tel.: +972 4 8292426; fax: +972 4 8295697.
E-mail address: cvolokh@technion.ac.il (K.Y. Volokh).

0020-7683/$ - see front matter © 2008 Elsevier Ltd. All rights reserved.
doi:10.1016/j.ijsolstr.2008.07.016

The applicability of the linearized theory to the rubbery state of material is less evident and more restrictive. Inspecting the list of references provided by Persson et al. (2005), it is easy to observe again that the number of works on cracks in rubber is very limited. The latter is especially surprising since, as the authors notice, "the breakdown of tires because of catastrophic rubber crack propagation results in much higher loss of capital and life than airplane accidents, but there is little awareness of this, probably because such events are much less spectacular than a major airplane accident".

To shed more light on initiation of crack propagation in rubber-like materials, we simulate Mode I failure of a cracked rubber sheet under the hydrostatic tension by using the softening hyperelasticity approach described in Section 2, which can handle both geometrical and material nonlinearities. Such an approach allows capturing the critical tension on the cracked plate, which corresponds to the onset of static instability. Thus, our theoretical study is essentially a series of numerical experiments. The numerical experiments are not affected by the problems accompanying the physical experiments and because of that they can be a valuable source of additional information. We plug the softening hyperelasticity models in ABAQUS and use very fine meshes to simulate small cracks with the varying sharpness or length in Section 3.

We find that the critical tension imposed on the rubber sheet is sensitive to the crack sharpness when the shear modulus is significantly greater than the average bond energy. The sensitivity declines when the shear modulus approaches the value of the value of the average bond energy. Roughly speaking, softer materials are less sensitive to cracks than more brittle materials where the brittleness is defined as a ratio of the shear modulus to the average bond energy. It is also found that the critical tension is proportional to the inverse square root of the crack length for more brittle materials. The latter means that the Griffith theory based on the linearized elasticity is also applicable to soft materials undergoing large deformations. Unfortunately, the applicability of the Griffith theory is restricted to cracks with the same sharpness only. We discuss results of our simulations and compare them to the predictions of LEFM in Section 4. The discussion focuses on the influence of the crack sharpness, i.e. the tip curvature, and the crack length on the onset of fracture in rubber.

2. Softening hyperelasticity

2.1. Continuum models of failure

The existing continuum mechanics approaches for modeling material failure can be divided in two groups: surface and bulk models. The surface models, pioneered by Barenblatt (1959), appear by name of cohesive zone models (CZMs) in the modern literature. They present material surfaces – cohesive zones – where displacement discontinuities occur. The discontinuities are enhanced with constitutive laws relating normal and tangential displacement jumps with the corresponding tractions. There is a plenty of proposals of constitutive equations for the cohesive zones: Dugdale (1960), Rice and Wang (1989), Tvergaard and Hutchinson (1992), Xu and Needleman (1994), Camacho and Ortiz (1996), for example. All CZM are constructed qualitatively as follows: tractions increase, reach a maximum, and then approach zero with increasing separation. Such a scenario is in harmony with our intuitive understanding of the rupture process. Since the work by Needleman (1987) CZM are used increasingly in finite element simulations of crack tip plasticity and creep; crazing in polymers; adhesively bonded joints; interface cracks in bimaterials; delamination in composites and multilayers; fast crack propagation in polymers, etc. Cohesive zones can be inside finite elements or along their boundaries (De Borst, 2001; Xu and Needleman, 1994; Belytschko et al., 2001). Crack nucleation, propagation, branching, kinking, and arrest are a natural outcome of the computations where the discontinuity surfaces are spread over the bulk material. This is in contrast to the traditional approach of fracture mechanics where stress analysis is separated from a description of the actual process of material failure. The CZM approach is natural for simulation of fracture at the *internal material interfaces* in polycrystals, composites, and multilayers. It is less natural for modeling fracture of the bulk because it leads to the simultaneous use of two material models for the same real material: one model describes the bulk while the other model describes CZM imbedded in the bulk. Such two-model approach is rather artificial physically. It seems preferable to incorporate a material failure law directly in the constitutive description of the bulk.

Remarkably, the first models of bulk failure – damage mechanics – proposed by Kachanov (1958) and Rabotnov (1963) for analysis of the gradual failure accumulation and propagation in *creep* and *fatigue* appeared almost simultaneously with the cohesive zone approach. The need to describe the failure *accumulation*, i.e. evolution of the material microstructure, explains why damage mechanics is very similar to plasticity theories including (a) the internal damage variable (inelastic strain), (b) the critical threshold condition (yield surface), and (c) the damage evolution equation (flow rule). The subsequent development of the formalism of damage mechanics (Kachanov, 1986; Krajcinovic, 1996; Skrzypek and Ganczarski, 1999; Lemaitre and Desmorat, 2005) left its physical origin well behind the mathematical and computational techniques and, eventually, led to the use of damage mechanics for the description of *any* bulk failure. Theoretically, the approach of damage mechanics is very flexible and allows reflecting physical processes triggering macroscopic damage at small length scales. Practically, the experimental calibration of damage theories is not trivial because it is difficult to measure the damage parameter directly. The experimental calibration should be implicit and include both the damage evolution equation and criticality condition.

A physically motivated alternative to damage mechanics in the cases of failure related with the bond rupture has been considered recently by Gao and Klein (1998), Klein and Gao (1998) who showed how to mix the atomic/molecular and continuum descriptions in order to simulate material failure. They applied the Cauchy–Born rule linking micro- and macroscales to empirical potentials, which include a possibility of the full atomic separation. The continuum–atomistic link led to the formulation of the macroscopic strain energy potentials allowing for the stress/strain softening and strain localization.

The continuum–atomistic method is very effective at small length scales where purely atomistic analysis becomes computationally intensive. Unfortunately, a direct use of the continuum–atomistic method in macroscopic failure problems is not very feasible because its computer implementation includes a numerically involved procedure of the averaging of the interatomic potentials over a representative volume.

In order to bypass the computational intensity of the continuum–atomistic method while preserving its sound physical basis the *softening hyperelasticity* approach was proposed by Volokh (2004, 2007). The basic idea of the approach was to formulate an expression of the stored macroscopic energy, which would include the energy limiter – the average bond energy or the failure energy. Such a limiter automatically induces strain softening, that is a material failure description, in the constitutive law. The softening hyperelasticity approach is computationally simple yet physically appealing and we describe it below.

2.2. Energy limiter

Let us start with the interaction of two particles (atoms, molecules, etc.) and let us choose, to be specific, the Lennard–Jones potential, φ, for the description of the particle interaction

$$\varphi(l) = 4\varepsilon((\sigma/l)^{12} - (\sigma/l)^{6}), \tag{1}$$

where l is the distance between particles ε and σ are the *bond energy* and length constants accordingly – Fig. 1.

Let L designate the distance between particles in a reference state and F be the one-dimensional deformation gradient. In the latter case we have

$$l = FL. \tag{2}$$

Substituting (2) in (1) we have

$$\varphi(F) = 4\varepsilon((\sigma/FL)^{12} - (\sigma/FL)^{6}). \tag{3}$$

Assuming that deformation increases to infinity we have

$$\varphi(F \to \infty) = 0. \tag{4}$$

On the other hand, we have at the reference state

$$\varphi_0 = \varphi(F = 1) = 4\varepsilon((\sigma/L)^{12} - (\sigma/L)^{6}). \tag{5}$$

In the absence of external loads the energy of the interaction tends to minimum and it is natural to choose the minimum energy state – equilibrium – at distance $L = \sqrt[6]{2}\sigma$ where no forces are acting between the particles. In the latter case, we have

$$\varphi_0 = -\varepsilon. \tag{6}$$

We notice that energy is negative in the equilibrium state according to the classical Lennard–Jones (LJ) potential. The latter is inconvenient in solid mechanics and we modify the classical LJ potential by shifting its reference energy to zero (Fig. 1)

$$\psi = \varphi + \varepsilon. \tag{7}$$

We further formalize the described energy shift as follows:

$$\psi(F) = \varphi(F) - \varphi_0, \tag{8}$$

$$\varphi_0 = \min_L \varphi(F = 1). \tag{9}$$

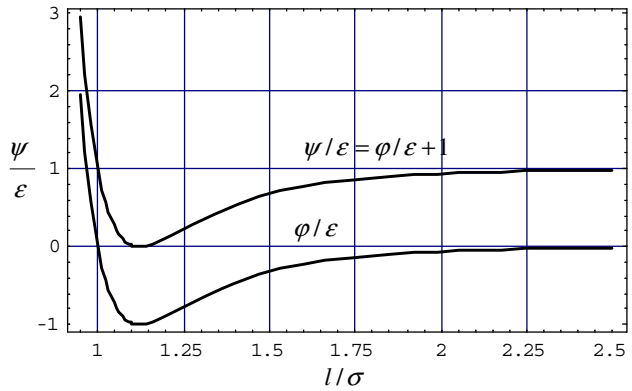

Fig. 1. Lennard–Jones potential.

Eqs. (8) and (9) are important in the subsequent consideration of assemblies of many particles.

It is important to emphasize that we cannot increase energy unlimitedly by increasing deformation. The energy increase is limited

$$\psi(F \to \infty) = -\varphi_0 = \Phi = \text{constant}. \tag{10}$$

Now we extend all considerations for a pair of particles given above to large assemblies of particles comprising solid bodies. Consider particles placed at $\mathbf{r}_i$ in the 3D space. Generally, the volumetric density of the total potential energy, i.e. the strain energy, can be written with account of two-particle interactions as follows:

$$\frac{1}{2V}\sum_{i,j}\varphi(r_{ij}), \tag{11}$$

where $r_{ij} = |\mathbf{r}_{ij}| = |\mathbf{r}_i - \mathbf{r}_j|$ and V is the volume occupied by the system.

According to the Cauchy–Born rule (Weiner, 1983; Tadmor et al., 1996), originally applied to the crystal elasticity, the current $\mathbf{r}_{ij}$ and initial (reference) $\mathbf{R}_{ij} = \mathbf{R}_i - \mathbf{R}_j$ relative positions of the same two particles can be related by the deformation gradient:

$$\mathbf{r}_{ij} = \mathbf{F}\mathbf{R}_{ij}, \tag{12}$$

where $\mathbf{F} = \partial\mathbf{x}/\partial\mathbf{X}$ is the deformation gradient of a generic material macro-particle of body Ω occupying position $\mathbf{X}$ at the reference state and position $\mathbf{x}(\mathbf{X})$ at the current state of deformation – Fig. 2.

Substituting (12) in (11) yields

$$\frac{1}{2V}\sum_{i,j}\varphi(r_{ij}) = \frac{1}{2V}\sum_{i,j}\varphi(r_{ij}(\mathbf{C})), \tag{13}$$

where $\mathbf{C} = \mathbf{F}^{\mathrm{T}}\mathbf{F}$ is the right Cauchy–Green deformation tensor.

Direct application of (13) to analysis of material behavior can be difficult because of the large amount of particles. Gao and Klein (1998) and Klein and Gao (1998) considered the following statistical averaging procedure:

$$\langle\varphi(l)\rangle = \frac{1}{V_0}\int_{V_0^*}\varphi(l)D_{\mathrm{V}}\,\mathrm{d}V, \tag{14}$$

$$l = r_{ij} = L\sqrt{\boldsymbol{\xi}\cdot\mathbf{C}\boldsymbol{\xi}} = L|\mathbf{F}\boldsymbol{\xi}|, \tag{15}$$

where $L = R_{ij} = |\mathbf{R}_i - \mathbf{R}_j|$ is the reference bond length; $\boldsymbol{\xi} = (\mathbf{R}_i - \mathbf{R}_j)/L$ is the reference bond direction; V_0 is the reference representative volume; $\varphi(l)$ is the bond potential (LJ); D_{V} is the volumetric bond density function; and V_0^* is the integration volume defined by the range of influence of φ.

Now the average strain energy takes the form

$$\langle\varphi(\mathbf{C})\rangle = \frac{1}{V_0}\int_{V_0^*} 4\varepsilon((\sigma/L\|\mathbf{C}\|)^{12} - (\sigma/L\|\mathbf{C}\|)^{6})D_{\mathrm{V}}\,\mathrm{d}V, \tag{16}$$

where

$$\|\mathbf{C}\| = \sqrt{\boldsymbol{\xi}\cdot\mathbf{C}\boldsymbol{\xi}}. \tag{17}$$

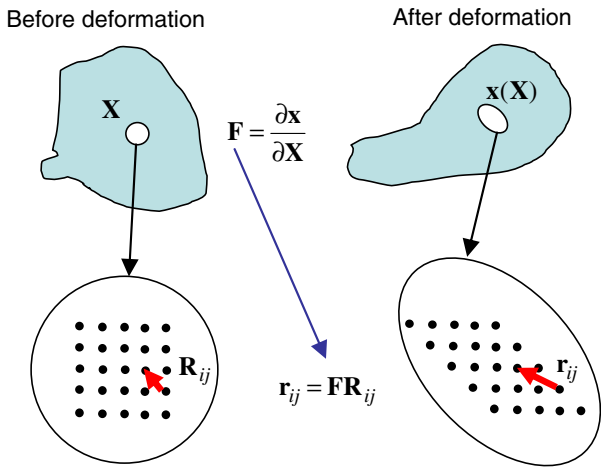

Fig. 2. Cauchy–Born rule.

Analogously to the case of the pair interaction considered in Section 2.1 – Eqs. (8) and (9) – we define the shifted strain energy, which is zero at the equilibrium reference state

$$\psi(\mathbf{C}) = \langle\varphi(\mathbf{C})\rangle - \langle\varphi\rangle_0, \tag{18}$$

$$\langle\varphi\rangle_0 = \min_L \langle\varphi(\mathbf{C} = \mathbf{1})\rangle. \tag{19}$$

Analogously to (10), we can define *the average bond energy* by setting the unlimited increase of deformation

$$\Phi = \psi(\|\mathbf{C}\| \to \infty) = -\langle\varphi\rangle_0 = \text{constant}. \tag{20}$$

Thus, *the average bond energy sets a limit for the energy accumulation*. This conclusion generally does not depend on the choice of the particle potential and it is valid for any interaction that includes a possible particle separation – the bond energy.

Contrary to the conclusion above traditional hyperelastic models of materials do not include the energy limiter. The stored energy of hyperelastic materials is defined as

$$\psi = W. \tag{21}$$

Here, W is used for the strain energy of the *intact* material, which can be characterized as follows:

$$\|\mathbf{C}\| \to \infty \Rightarrow \psi = W \to \infty, \tag{22}$$

where $\|\ldots\|$ is a tensorial norm.

In other words, the increasing strain increases the accumulated energy unlimitedly. Evidently, the consideration of only intact materials is restrictive and unphysical. The energy increase of a real material should be limited as it is shown above:

$$\|\mathbf{C}\| \to \infty \Rightarrow \psi \to \Phi = \text{constant}, \tag{23}$$

where the average bond energy, $\Phi = \text{constant}$, can be called the *material failure energy*.

Eq. (23) presents the fundamental idea of introducing a limiter of the stored energy in the elasticity theory. Such a limiter induces material softening, indicating material failure, automatically. *The choice of the limited stored energy expression should generally be material-specific*. Nonetheless, a somewhat universal formula (Volokh, 2007) can be introduced to enrich the already existing models of intact materials with the failure description

$$\psi(W) = \Phi - \Phi\exp(-W/\Phi). \tag{24}$$

where $\psi(W = 0) = 0$ and $\psi(W = \infty) = \Phi$.

Formula (24) obeys condition $\|\mathbf{C}\| \to \infty \Rightarrow \psi(W(\mathbf{C})) \to \Phi$ and, in the case of the intact material behavior, $W \ll \Phi$, we have $\psi(W) \approx W$ preserving the features of the intact material.

The constitutive equation can be written in the general form accounting for (24)

$$\boldsymbol{\sigma} = 2J^{-1}\mathbf{F}\frac{\partial\psi}{\partial\mathbf{C}}\mathbf{F}^{\mathrm{T}} = 2J^{-1}\mathbf{F}\frac{\partial W}{\partial\mathbf{C}}\mathbf{F}^{\mathrm{T}}\exp\left(-\frac{W}{\Phi}\right), \tag{25}$$

where $\boldsymbol{\sigma}$ is the Cauchy stress tensor; $J = \det\mathbf{F}$; and the exponential multiplier enforces material softening. Constitutive equation (25) is especially effective for incompressible soft materials undergoing finite deformations. We strongly emphasize again that the best form of the energy function can be material/problem-specific.

2.3. Neo-Hookean material with softening

The neo-Hookean intact material is the simplest model for rubber-like solids, which can be obtained as a limit case for many more sophisticated theories. The stored energy of the incompressible neo-Hookean solid is defined as follows:

$$W(I_1) = \frac{\alpha}{2}(I_1 - 3). \tag{26}$$

Here, α is the shear modulus and $I_1 = \mathrm{tr}\,\mathbf{C} = \mathrm{tr}\,\mathbf{B}$ is the first principal invariant of with softening, where $\mathbf{C} = \mathbf{F}^{\mathrm{T}}\mathbf{F}$ and $\mathbf{B} = \mathbf{F}\mathbf{F}^{\mathrm{T}}$ are the right and the left Cauchy–Green deformation tensors accordingly.

We enhance this model with softening following (24) and (25):

$$\psi = \Phi - \Phi\exp\left(-\frac{\alpha}{2\Phi}(I_1 - 3)\right), \tag{27}$$

$$\boldsymbol{\sigma} = -p\mathbf{1} + \alpha\mathbf{B}\exp\left(-\frac{\alpha}{2\Phi}(I_1 - 3)\right), \tag{28}$$

where p is pressure-like Lagrange multiplier enforcing the incompressibility condition

$$J = \det\mathbf{F} = 1 = \det\mathbf{B}. \tag{29}$$

To clarify the physical meaning of the model, we consider the case of uniaxial tension, which can be used for the model calibration in tests:

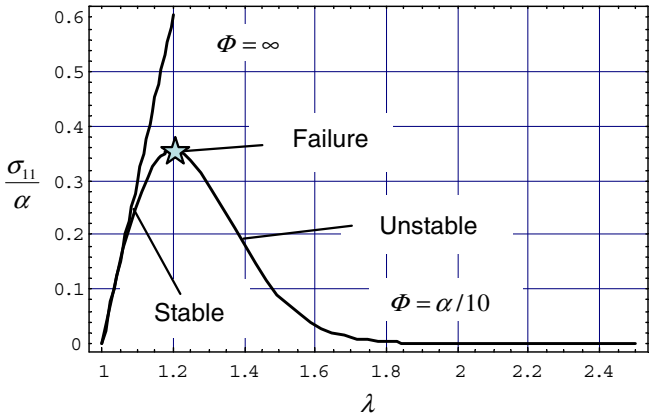

Fig. 3. Uniaxial tension of the neo-Hookean material with and without softening.

$$x_1 = \lambda X_1, \quad x_2 = \lambda^{-1/2} X_2, \quad x_3 = \lambda^{-1/2} X_3, \tag{30}$$

$$\mathbf{B} = \lambda^2 \mathbf{e}_1 \otimes \mathbf{e}_1 + \lambda^{-1}(\mathbf{e}_2 \otimes \mathbf{e}_2 + \mathbf{e}_3 \otimes \mathbf{e}_3), \tag{31}$$

$$\sigma_{11} = \alpha(\lambda^2 - \lambda^{-1}) \exp\left(-\frac{\alpha}{2\Phi}(\lambda^2 + 2\lambda^{-1} - 3)\right), \tag{32}$$

where λ designates the axial stretch.

The stress–stretch curve described by (32) is shown in Fig. 3. The maximum point on the curve with the finite average bond energy indicates the onset of the material failure/rupture. When the stretch reaches the maximum, no stable solution of the static problem exists and the failure starts propagating.

We use the softening neo-Hookean material for simulating the onset of fracture in a rubber sheet in the following section.

Remark 2.1. The so-called Cauchy–Born rule linking micro- and macro-scales was originally formulated for crystal elasticity and it is widely used in modern continuum–atomistic methods. The Cauchy–Born rule is essentially an assumption of affinity of deformation of the physical particles within the representative small volumes of material. The applicability of the affinity hypothesis implies the applicability of the classical (local) continuum mechanics description of material. The continuum description of material proved itself for most materials at large length scales. It may fail, however, at small length scales where, for example, the atomic relaxation cannot be ignored. The latter cases are out of our consideration and we always assume that the local deformation is approximately affine.

Remark 2.2. It is important to realize that not all bonds between the material particles are of equal importance in (14). Only bonds presenting the weakest links define failure. In this sense, it is probably better to call the energy limiter the *failure energy* rather than the average bond energy.

Remark 2.3. To illustrate the capability of the proposed approach to describe failure, we present an example of the experimental calibration of the material of the abdominal aortic aneurysm (AAA). AAA is rubber-like and its stored energy with softening can be written based on (25) as follows (Volokh and Vorp, 2008): $\psi(I_1) = \Phi - \Phi \exp(-\alpha_1(I_1 - 3)/\Phi - \alpha_2(I_1 - 3)^2/\Phi)$, where $I_1 = \mathrm{tr}\mathbf{C}$; α_1 and α_2 are the elasticity constants of the material; and Φ is the failure energy. The uniaxial tension test results are shown in Fig. 4, where the model was fitted with the following constants: $\alpha_1 = 10.3$ N/cm^2; $\alpha_2 = 18.0$ N/cm^2; $\Phi = 40.2$ N/cm^2.

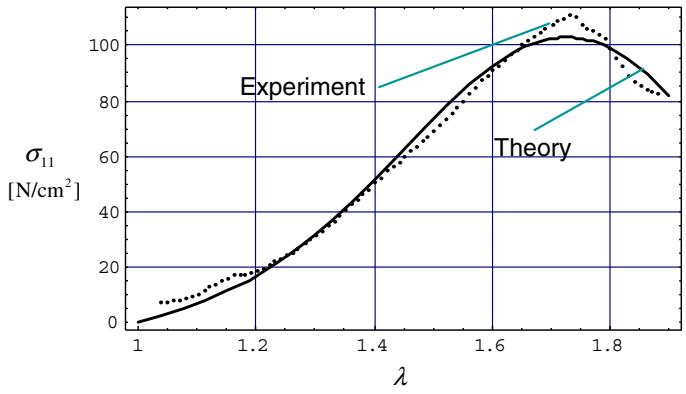

Fig. 4. Theory versus experiment for the uniaxial tension test of AAA (Volokh and Vorp, 2008).

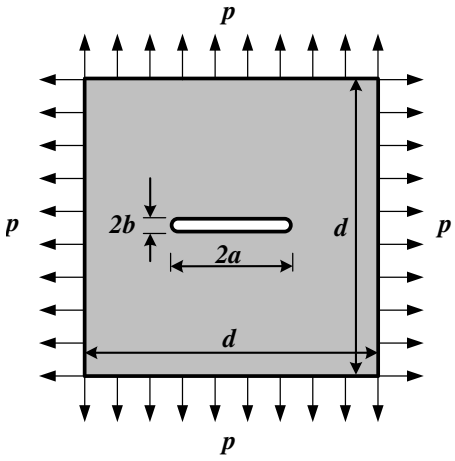

Fig. 5. Crack in a rubber sheet under hydrostatic tension.

3. Finite element analysis

The purpose of the finite element analysis is to simulate transition to failure of a thin rubber sheet with a small crack under the hydrostatic tension – Fig. 5.

For this purpose, we plug the strain energy function (27) in ABAQUS (2007). We consider the state of the plane stress for a square sheet of size $d = 1600$ (units) with varying brittleness, i.e. ratio of the shear modulus to the average bond energy: $\alpha/\Phi = 0.1, 1.0, 10.0, 100.0$. To capture the stress/strain concentration at the tip of the crack, we use very fine meshes as illustrated in Fig. 6. The number of elements varies in computations to ensure convergence of the results.

We calculate the critical load of the onset of static structural (global) instability by using the ABAQUS procedure for the equilibrium path tracing. The critical load corresponds to the maximum tension that the rubber sheet can bear before the crack propagation starts.

We start with simulations of the crack with fixed length of $2a = 80$ (units) and varying sharpness: $b = 0.5, 1.0, 1.5, 2.0, 2.5, 3.0, 3.5, 4.0$ (units). Table 1 presents the normalized critical tension for eight cases of the crack sharpness.

Every case is simulated with two different meshes to check the convergence. The results are very similar in both cases and their average is presented in Fig. 7 graphically.

It is clearly seen that the critical tension significantly depends on the crack sharpness for more brittle rubbers. Such dependence declines when rubbers get softer.

In addition to analysis of the influence of the crack sharpness on the critical tension in the rubber sheet, it is of interest to compare cracks with the equivalent sharpness and varying length and brittleness – Fig. 8.

The obtained data show that the critical tension depends on the crack length. Moreover, it turns out that the critical tension is inversely proportional to the square root of the crack length resembling the famous Griffith (1921) finding and the following formula of LEFM:

$$p_{cr} = \frac{K_{Ic}}{\sqrt{\pi a}}, \tag{33}$$

where K_{Ic} is the fracture toughness.

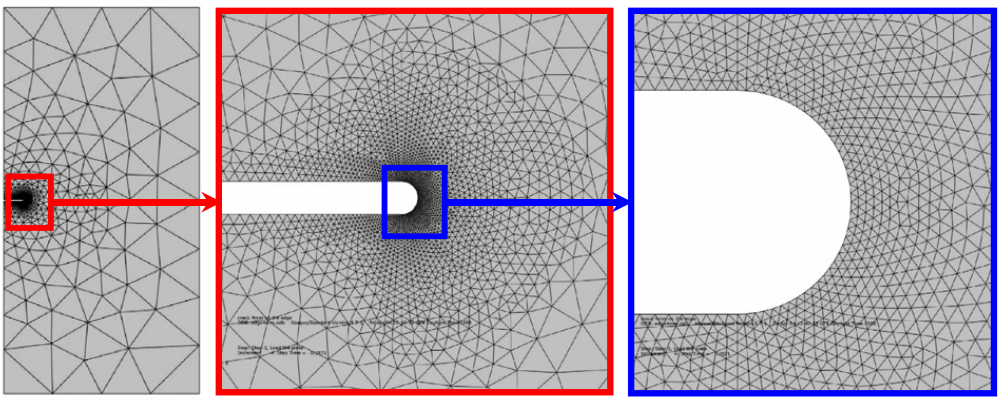

Fig. 6. Sample finite element mesh.

Table 1
Normalized critical tension, p_{cr}/Φ, for crack with varying sharpness and rubber sheet with varying brittleness, α/Φ (second numbers designate the number of finite elements)

b/a	α/Φ							
	0.1		1		10		100	
0.5/40	33×10^{-3}	33×10^{-3}	10×10^{-2}	10×10^{-2}	35×10^{-2}	35×10^{-2}	10×10^{-1}	10×10^{-1}
	1296	1738	1296	1738	1296	1738	1296	1738
1.0/40	44×10^{-3}	45×10^{-3}	15×10^{-2}	16×10^{-2}	47×10^{-2}	47×10^{-2}	15×10^{-1}	15×10^{-1}
	1764	3624	1764	3624	1764	3624	1764	3624
1.5/40	52×10^{-3}	53×10^{-3}	18×10^{-2}	19×10^{-2}	56×10^{-2}	57×10^{-2}	17×10^{-1}	18×10^{-1}
	1366	2694	1366	2694	1366	2694	1366	2694
2.0/40	56×10^{-3}	57×10^{-3}	20×10^{-2}	21×10^{-2}	64×10^{-2}	65×10^{-2}	20×10^{-1}	20×10^{-1}
	1382	2546	1382	2546	1382	2546	1382	2546
2.5/40	61×10^{-3}	62×10^{-3}	22×10^{-2}	23×10^{-2}	72×10^{-2}	73×10^{-2}	22×10^{-1}	23×10^{-1}
	1338	2268	1338	2268	1338	2268	1338	2268
3.0/40	64×10^{-3}	65×10^{-3}	24×10^{-2}	25×10^{-2}	77×10^{-2}	79×10^{-2}	24×10^{-1}	25×10^{-1}
	2262	4040	2262	4040	1326	2262	2262	4040
3.5/40	67×10^{-3}	68×10^{-3}	26×10^{-2}	27×10^{-2}	83×10^{-2}	84×10^{-2}	25×10^{-1}	26×10^{-1}
	1274	2298	1274	2298	1274	2298	1274	2298
4.0/40	69×10^{-3}	70×10^{-3}	27×10^{-2}	28×10^{-2}	88×10^{-2}	89×10^{-2}	26×10^{-1}	27×10^{-1}
	1274	2368	1274	2368	1274	2368	1274	2368

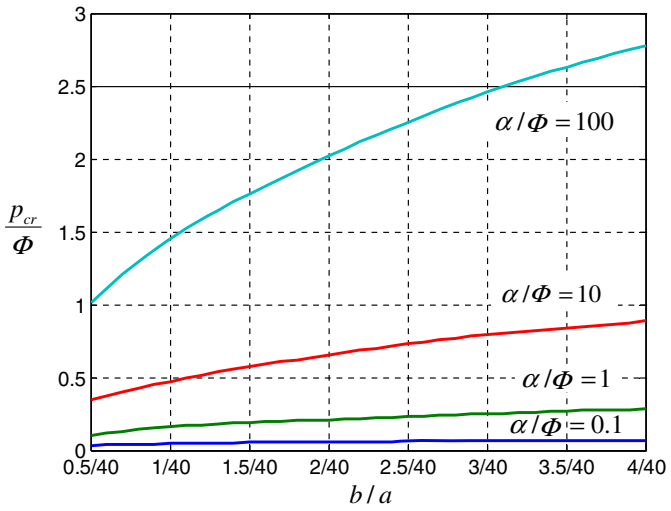

Fig. 7. Normalized critical tension, p_{cr}/Φ, for crack with varying sharpness and rubber sheet with varying brittleness, α/Φ.

To make comparison between our calculations and the classical theory of brittle fracture described by (33), we calibrated the fracture toughness for $a/b = 40/2$ and drew the graphs of Griffith/LEFM solutions in Fig. 8. Evidently, the more brittle rubbers are described reasonably well by the classical theory of brittle fracture for equivalent cracks, i.e. cracks with the same sharpness, b = constant, as the one calibrated in experiments. Unfortunately, the calibration of the fracture toughness is not unique and it depends on the crack sharpness as it is seen in Fig. 8. In the case of softer materials – bottom of Fig. 8 – LEFM does not work well.

Softer materials are less sensitive to the crack sharpness because they undergo large deformations at the tip of the crack. To illustrate this point, we superimpose and compare finite element meshes at the beginning of loading and at the critical load – Fig. 9.

Evidently, huge deformations can develop around the crack for softer materials. As a result of that the failure can occur before the tension reaches the critical value predicted by LEFM as shown on the bottom of Fig. 8.

4. Discussion

In the present work, we studied the influence of large deformations on the initiation of crack propagation in rubber-like materials. Specifically, we considered a sheet of the neo-Hookean incompressible material with a central crack under hydrostatic tension. The critical tension of the fracture initiation occurs when material fails at the tip of the crack. The failure is driven by the strain softening induced in the material constitutive model with the help of the energy limiter – the average bond energy. The neo-Hookean model enhanced with the failure description was plugged in ABAQUS and crack simulations

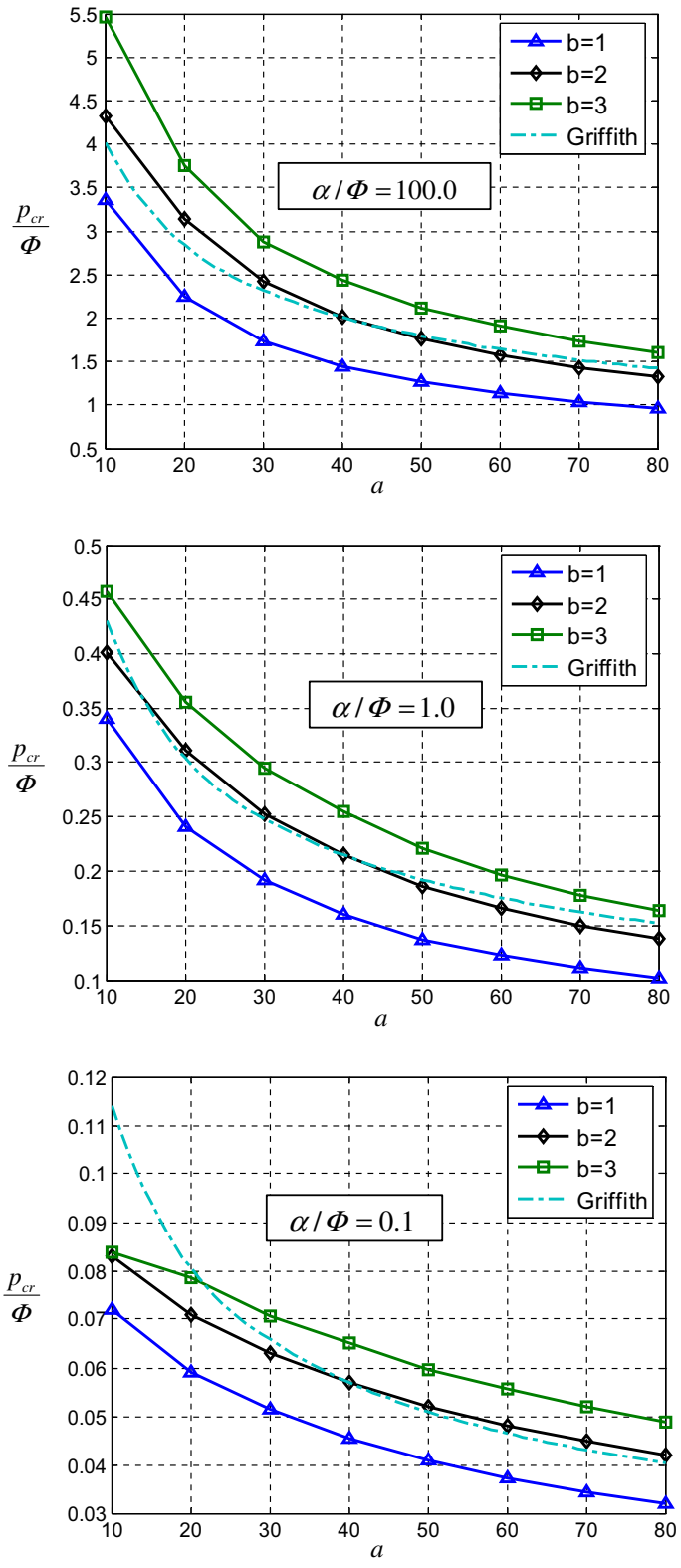

Fig. 8. Critical tension for cracks with varying lengths, sharpness, and brittleness; Griffith – prediction based on Eq. (33) for K_{Ic} is calibrated at $a/b = 40/2$.

were performed on very fine meshes to examine the influence of the crack length, sharpness, and the material brittleness on the onset of fracture. It was observed that lower magnitudes of the critical tension were driven by

(i) sharper cracks;
(ii) lengthier cracks;
(iii) lower brittleness, i.e. the ratio of the shear modulus to the average bond energy.

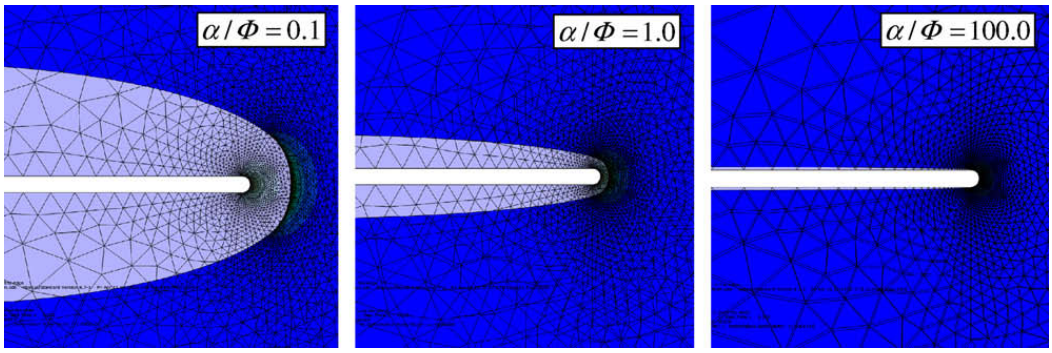

Fig. 9. Finite element meshes at the initial (gray) and the critical (blue) states at the tip of the crack ($a = 40;\ b = 1$) for the increasing brittleness ratio. (For interpretation of color mentioned in this figure the reader is referred to the web version of the article.)

Factors (i) and (ii) directly echo the classical theories of brittle fracture – see also Volokh and Trapper (2008). Factor (iii) is more specific of soft materials undergoing large deformations.

Our observations on the role of the crack sharpness are in agreement with the well-known Inglis (1913) finding that the stress at the tip of an elliptic crack strongly depends on its sharpness. Assuming that the stress at the tip controls material strength, it is possible to expect that the crack sharpness affects the onset of material failure. Such a scenario was considered by Inglis using *linear* elasticity. Recently, Emmerich (2007) revisited Inglis results by mixing continuum and atomistic arguments and arriving at similar conclusions. It is interesting to note that the Griffith theory and LEFM are ignorant of the crack sharpness because they are based on the energy balance considerations, which are integral and because of that they 'smear' the real stress/strain concentration at the tip of a real crack (Volokh and Trapper, 2008).

Our observations on the role of the crack length are in a *partial* agreement with LEFM. Our simulations of the straight cracks show that the critical tension depends approximately inversely on the square root of the crack length in full harmony with the Griffith finding. Unfortunately, that is true only for the equivalent cracks, i.e. cracks with the same tips.

Our observations on the role of the material brittleness strongly suggest that the decrease of the shear modulus as compared to the average bond energy leads to a decline of the material sensitivity to a crack-like flow. This means, specifically, that the dependence of the critical load on the crack length and sharpness is less pronounced in softer materials than in more brittle ones. The latter happens because softer materials can undergo large deformations 'suppressing' the stress/strain concentration. In other words, softer materials 'absorb' the high stresses/strains at the tip of the crack due to large deformations. To avoid confusions, however, we strongly emphasize that though softer materials are less sensitive to the crack length and sharpness they tear under lower critical loads than more brittle materials. The latter point should not be overlooked by a reader.

References

ABAQUS, Version 6.7-1, 2007. H.K.S Inc., Pawtucket, RI.
Barenblatt, G.I., 1959. The formation of equilibrium cracks during brittle fracture. General ideas and hypotheses. Axially-symmetric cracks. J. Appl. Math. Mech. 23, 622–636.
Belytschko, T., Moes, N., Usiu, S., Parimi, C., 2001. Arbitrary discontinuities in finite elements. Int. J. Numer. Meth. Eng. 50, 993–1013.
Camacho, G.T., Ortiz, M., 1996. Computational modeling of impact damage in brittle materials. I. J. Solids Struct. 33, 2899–2938.
De Borst, R., 2001. Some recent issues in computational failure mechanics. Int. J. Numer. Meth. Eng. 52, 63–95.
Dugdale, D.S., 1960. Yielding of steel sheets containing slits. J. Mech. Phys. Solids 8, 100–104.
Emmerich, F.G., 2007. Tensile strength and fracture toughness of brittle materials. J. Appl. Phys. 102, 073504.
Gao, H., Klein, P., 1998. Numerical simulation of crack growth in an isotropic solid with randomized internal cohesive bonds. J. Mech. Phys. Solids 46, 187–218.
Gent, A.N. (Ed.), 2001. Engineering with Rubber: How to Design Rubber Components. Hanser, Munich.
Geubelle, P.H., 1995. Finite deformation effects in homogeneous and interfacial fracture. Int. J. Solids Struct. 32, 1003–1016.
Geubelle, P.H., Knauss, W.G., 1994a. Finite strain at the tip of the crack in a sheet of hyperelastic material: homogeneous case. J. Elasticity 35, 61–98.
Geubelle, P.H., Knauss, W.G., 1994b. Finite strain at the tip of the crack in a sheet of hyperelastic material: special bimaterial cases. J. Elasticity 35, 99–137.
Geubelle, P.H., Knauss, W.G., 1994c. Finite strain at the tip of the crack in a sheet of hyperelastic material: general bimaterial case. J. Elasticity 35, 138–174.
Griffith, A.A., 1921. The phenomena of rupture and flow in solids. Philos. Trans. Roy. Soc. London A 221, 163–198.
Herrmann, J.M., 1989. An asymptotic analysis of finite deformation near tip of an interface crack. J. Elasticity 21, 227–269.
Inglis, C.E., 1913. Stresses in a plate due to presence of cracks and sharp corners. Proc. Inst. Naval Architects 55, 219–241.
Kachanov, L.M., 1958. Time of the rupture process under creep conditions. Izvestiia Akademii Nauk SSSR, Otdelenie Teckhnicheskikh Nauk 8, 26–31.
Kachanov, L.M., 1986. Introduction to Continuum Damage Mechanics. Martinus Nijhoff, Dotrecht, Netherlands.
Klein, P., Gao, H., 1998. Crack nucleation and growth as strain localization in a virtual-bond continuum. Eng. Fract. Mech. 61, 21–48.
Knowles, J.K., 1977. The finite anti-plane shear field near the tip of a crack for a class of incompressible elastic solids. Int. J. Fract. 13, 611–639.
Knowles, J.K., 1981. A nonlinear effect in mode II crack problems. Eng. Fract. Mech. 15, 469–476.
Knowles, J.K., Sternberg, E., 1973. An asymptotic finite-deformation analysis of the elastostatic field near the tip of the crack. J. Elasticity 3, 67–107.
Knowles, J.K., Sternberg, E., 1983. Large deformations near the tip of an interface crack between two neo-Hookean sheets. J. Elasticity 13, 257–293.
D. Krajcinovic, Damage Mechanics, North-Holland Series in Applied Mathematics and Mechanics. Elsevier, Amsterdam, 1996.
Lemaitre, J., Desmorat, R., 2005. Engineering Damage Mechanics: Ductile, Creep, Fatigue and Brittle Failures. Springer, Berlin.
Needleman, A., 1987. A continuum model for void nucleation by inclusion debonding. J. Appl. Mech. 54, 525–531.
Persson, B.N., Albohr, O., Heinrich, G., Ueba, H., 2005. Crack propagation in rubber-like materials. J. Phys.: Cond. Matter. 17, R1071–R1142.

Rabotnov, Y.N., 1963. On the equations of state for creep. In: Progress in Applied Mechanics (Prager Anniversary Volume). MacMillan, New York.
Rice, J.R., Wang, J.S., 1989. Embrittlement of interfaces by solute segregation. Mater. Sci. Eng. A 107, 23–40.
Skrzypek, J., Ganczarski, A., 1999. Modeling of Material Damage and Failure of Structures. Springer, Berlin.
Tadmor, E.B., Ortiz, M., Phillips, R., 1996. Quasicontinuum analysis of defects in solids. Philos. Mag. 73, 1529–1563.
Tvergaard, V., Hutchinson, J.W., 1992. The relation between crack growth resistance and fracture process parameters in elastic–plastic solids. J. Mech. Phys. Solids 40, 1377–1397.
Volokh, K.Y., 2004. Nonlinear elasticity for modeling fracture of isotropic brittle solids. J. Appl. Mech. 71, 141–143.
Volokh, K.Y., 2007. Hyperelasticity with softening for modeling materials failure. J. Mech. Phys. Solids 55, 2237–2264.
Volokh, K.Y., Trapper, P., 2008. Fracture toughness from the standpoint of softening hyperelasticity. J. Mech. Phys. Solids 56, 2459–2472.
Volokh, K.Y., Vorp, D.A., 2008. A model of growth and rupture of abdominal aortic aneurysm. J. Biomech. 41, 1015–1021.
Weiner, J.H., 1983. Statistical Mechanics of Elasticity. Wiley, New York.
Xu, X.P., Needleman, A., 1994. Numerical simulations of fast crack growth in brittle solids. J. Mech. Phys. Solids 42, 1397–1434.